JAVMA

AVMA

Accuracy of virtual surgical planning and custom three-dimensionally printed osteotomy and reduction guides for acute uni- and biapical correction of antebrachial deformities in dogs

Christina C. De Armond, MVB, MS[1]; Daniel D. Lewis, DVM[1]*; Stanley E. Kim, BVSc, MS[1]; Adam H. Biedrzycki, BVSc, PhD[2]

[1]Department of Small Animal Clinical Sciences, College of Veterinary Medicine, University of Florida, Gainesville, FL
[2]Department of Large Animal Clinical Sciences, College of Veterinary Medicine, University of Florida, Gainesville, FL

*Corresponding author: Dr. Lewis (lewisda@ufl.edu)

https://doi.org/10.2460/javma.21.09.0419

OBJECTIVE
To report clinical experience using virtual surgical planning (VSP) and surgical application of 3D printed custom surgical guides to facilitate uni- and biapical correction of antebrachial deformities in dogs.

ANIMALS
11 dogs (13 antebrachial deformity corrections).

PROCEDURES
Using CT-based bone models, VSP was performed, and surgical guides were designed and 3D printed. The guides were used to execute osteotomies and align bone segments. Postoperative CTs were obtained to compare limb alignment with the VSP. Long-term assessment of lameness and cosmesis were compared with preoperative status.

RESULTS
Guides were successfully utilized and postoperative analysis was available for 10 of 13 deformities. Guides were abandoned in 2 deformities due to soft tissue tension. Evaluation of postoperative frontal, sagittal, axial, and translational limb alignment revealed that over 90% of parameters were within the acceptable range of ≤ 5° angulation and rotation or ≤ 5 mm of translation from the VSP. Lameness scores were improved in 7/8 deformities with associated preoperative lameness, and posture was improved in 10/10 deformities in which guides were deployed. Complications included reduced range of carpal motion (n = 2), implant sensitivity (n = 2), fracture (n = 1), and tendon laceration (n = 1).

CLINICAL RELEVANCE
VSP and customized surgical guide application facilitated accurate antebrachial limb deformity correction in the majority of deformities in this case series. The use of VSP and 3D printed guides would appear to be a viable and accurate approach for correction of both uni- and biapical antebrachial deformities in dogs.

Surgical management of antebrachial deformities in dogs has evolved over the past 4 decades.[1–11] Accurate characterization of the deformity and precise surgical execution are required for an optimal outcome.[2–16] Marked deformity, particularly rotational deformity, complicates surgical planning, especially when utilizing 2D imaging.[12,15,17,18] In addition, accurate execution of the preoperative plan can be technically challenging during the procedure.[8,10,11]

Computer-aided surgical planning and 3D printed custom surgical guides have been used to overcome these challenges.[8,11,18–28] Custom surgical guides facilitate the management of complex fractures, arthrodeses, and vertebral stabilization in dogs.[20,21,23–25,27] Virtual surgical planning (VSP) uses cross-sectional imaging of the area of interest and computer design software to plan and rehearse a surgery with or without the use of custom surgical guides to aid in the execution of the plan. VSP and custom guides have utility in planning and executing deformity correction. In human patients, custom osteotomy guides enable excellent clinical results in correction of malunited forearm fractures.[19] Custom osteotomy guide use also increases surgical accuracy and reduces fluoroscopy use during procedures to address valgus knee malalignment in human patients.[26] Disadvantages of VSP and custom guide use include the need for advanced specialized training, increased preoperative planning time, and the cost of software and required printing equipment.[29–31] Use of VSP and custom guides has been reported for the correction of antebrachial and femoral deformities in dogs, but this emerging surgical modality is novel and is rapidly evolving, and previous reports have only described uniapical correction.[8,11,18,22,28]

The objective of this retrospective study was to describe our methods for VSP as well as the design, printing, and application of custom osteotomy and reduction guides for uni- and biapical antebrachial deformity corrections in dogs. We evaluated the accuracy of executing the preoperative plan and assessed the clinical outcomes in dogs with antebrachial deformity treated with VSP and custom printed surgical guides.

Materials and Methods

The medical records of dogs that had antebrachial deformity corrections based on VSP and acute corrective surgery using 3D printed custom osteotomy and reduction guides performed at our institution between May 1, 2018, and August 2020 were reviewed. The steps for creating guides included image acquisition, image processing, transection at the level of the virtual center of rotation of angulation (CORA), reduction and osteotomy guide design, and guide printing and sterilization.

Clinical assessment

All dogs were assigned preoperative functional scores for the surgical limbs; this score was the sum of both a lameness score and a conformational and posture score. A lameness score was assigned as follows: none (0), subtle weight-bearing lameness (1), obvious weight-bearing lameness (2), intermittently non–weight-bearing lameness (3), or consistently non–weight-bearing lameness (4). Limb conformation and posture when sitting, standing, or ambulating was graded as follows: (0) normal conformation and posture, (1) mild conformational or intermittent mild postural abnormalities, (2) mild conformational or consistent postural abnormalities, (3) obvious conformational or consistent postural abnormalities, or (4) severe conformational or consistent postural abnormalities.

Imaging

All dogs underwent preoperative CT imaging (160-Slice Toshiba Aquillion CT Scanner; Cannon Medical Systems) of both thoracic limbs including the distal third of the humerus to the third phalanxes of the manus. Helical volume data with slice thickness of 0.5 mm and 0.3 mm slice overlap were acquired in a bone algorithm. Additional radiographs of the antebrachii were obtained at the discretion of the surgeon.

Image processing

Bone algorithm Digital Imaging and Communications in Medicine (DICOM) images were used to enable segmentation (Mimics medical imaging software suite; Materialise) of relevant osseous structures. Following segmentation, 3D parts were generated and exported as 3D standard-tessellation language files (stl) files to 3D medical imaging modeling software for VSP and custom guide design (3Matic; Materialise).

Virtual CORA-based transection

Deformities were characterized as uniapical or biapical by identifying the location of the single or multiple CORAs.[6] In unilaterally affected dogs, the VSP was guided by manually aligning the affected limb with a mirror image of the unaffected contralateral limb. Once the location of the CORA was identified, an osteotomy plane was created transverse to the radial anatomic axis at the level of the CORA, and both the radius and ulna were virtually transected using the plane, generating proximal and distal virtual segments. In dogs with biapical deformities, the osteotomy at the proximal CORA was performed first. CORAs were defined near to the elbow or carpus, resulting in a very short proximal or distal radial segment that would limit appropriate implant placement. In these instances, the osteotomy plane was translated distally or proximally to increase the length of the juxta-articular radial segments **(Figure 1)**.

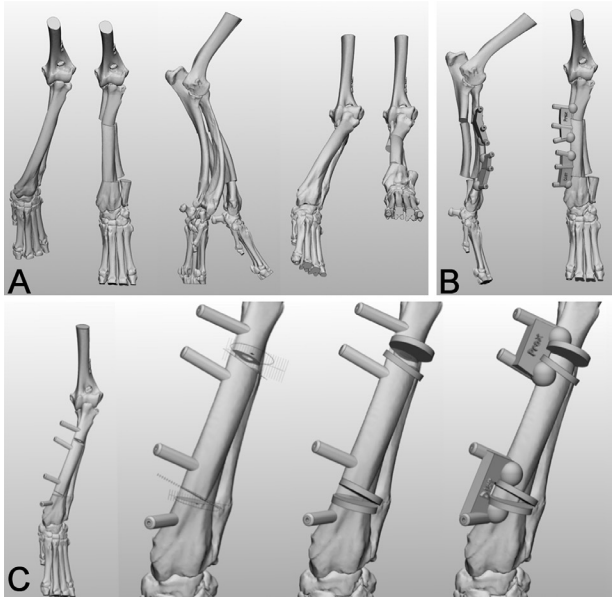

Figure 1—Images depicting correction of deformity 7 of a dog with an antebrachial deformity of this report. A—Initial virtual surgical planning for a biapical deformity correction (deformity 7). The radius and ulna have been transected at the proximal center of rotation of angulation and remote to the distal center of rotation of angulation. The distal segments have been manipulated in all planes until the metacarpus is aligned with the humeral condyle. B—Medial and dorsal projections of the corrected antebrachium (deformity 7). Reduction guides have been designed for each osteotomy using parallel drill guide towers and an additional converging drill guide tower. Note that the guide conforms precisely to the proximal and distal segments at the osteotomy and is designed to aid in translation of segments according to the virtual surgical planning. C—Design of osteotomy guides (deformity 7). The drill guide towers have been attached to the underlying bone segments of the virtually corrected antebrachium, and overlapping bone is removed. The drill guide tower and bone segments are then translated to their location on the precorrected limb. The resultant gaps between the bone segments are used to create osteotomy planes. Osteotomy shelves are created on the osteotomy planes. Note the completed osteotomy guides with material added to articulate individual components and conform to bone topography.

After the virtual osteotomy was performed, the distal segment (including the radius, ulna, and manus) was subjectively manipulated in frontal, sagittal, and axial planes until the desired correction was achieved by longitudinal alignment of the elbow and carpus. The correction resulted in overlapping bone between the proximal and distal segments that was removed from the nonjuxta-articular segment, creating closing wedge ostectomies. If the osteotomy planes were positioned remote to the CORA due to proximity to the elbow or carpus, the distal segment was translated medially or laterally to align the carpus and manus with the elbow. Desired correction and alignment were visually verified by manipulating the virtually corrected distal limb in all planes. Joint orientation angles were not measured on the corrected limb; correction was based on subjective appearance (Figure 1).

Reduction guides

Reduction guides were designed using the virtually corrected limb.[32] Two or 3 cannulated drill guides were constructed to fit on each radial segment on the virtually corrected limb and accommodate Kirschner wires of appropriate diameter. The drill guides adjacent to osteotomies were coplanar, allowing the reduction guide to slide into place. Additional drill guides located most distant to the osteotomy were angulated 20° to 45°, creating a converging angle with the parallel guides to stabilize the reduction once the Kirschner wires were placed. This construct allowed the reduction guide to seat securely on the bone surface without using threaded pins. A base was added, articulating the drill sleeves, which conformed to the virtual topography of the bone, particularly at the cut surface of proximal and distal segments. The contact between the bone and guide base aided in achieving a deliberate translational step or rotational correction (Figure 1).

Osteotomy guides

Osteotomy guides were also designed using the virtually corrected radius. The distal radial segments of the corrected virtual surgery model with the attached drill guide sleeves were translated and superimposed on the 3D image of the deformed radius. Osteotomy planes were created extending away from the osteotomy surface of each translated bone segment. The planes were used to create osteotomy shelves that were extended at least 1.5 cm cranially and/or medially from the radial cortex, providing a surface to guide a saw blade while creating the osteotomy. Bases connecting the osteotomy shelves and drill sleeves conformed to the topography of the preoperative radius. Guides were designed allowing assessment of the guide-bone interface at multiple locations. Location of guides ensured that unique osseous topography was incorporated at the guide-bone interface despite the minimalist footprint. This often included the region of the distal physeal scar and wrapping the guide caudally in the radial diaphysis (Figure 1).

Printing and sterilization

Models of the deformed and virtually corrected limb segments as well as the osteotomy and reduction guides were printed using a fused deposition modeler 3D printer (Fortus 450mc; Stratasys). Objects were printed using biocompatible plastics including PC-Iso (polycarbonate ISO) or ABS M30i (acetyl-butyl-styrene) based on material availability (Stratasys). Models were sterilized prior to surgery using ethylene oxide gas sterilization.

Surgery

Dogs were positioned in dorsal recumbency. A craniomedial approach to the radius was made, extending sufficiently proximal and distal to accommodate the osteotomy guides.[33] Guides were applied to the radius and secured using Kirschner wires. Positioning of the guides in the planned location was confirmed by observing congruency between the guide and the osseous topography as well as using printed bone models for reference. Osteotomies were made using a battery-operated drill (Colibri II; DePuy Synthes) with a sagittal saw attachment. The saw blade was maintained in direct contact with the osteotomy shelves to ensure accuracy of the osteotomy. An approach was made to the caudal (proximal) or lateral (distal) aspect of the ulna adjacent to each radial ostectomy site. Ulnar osteotomies or ostectomies were performed without using printed guides. The radial osteotomy guides were removed without removing the Kirschner wires adjacent to osteotomies; convergent wires were transiently removed. The radius was manipulated to oppose the osteotomy margins and position the implanted Kirschner wires parallel to each other. The guides were slid down the Kirschner wires until they were in direct contact with the radial cortex, thereby aligning and reducing the radial segments. Convergent wires were replaced. Appropriate reduction and alignment were confirmed by comparing the surgical limb with the printed corrected model. Reduction forceps (LCP toothed reduction forceps; DePuy Synthes) were applied to compress the reduction guide to the surface of the radius, and additional Kirschner wires were placed through the remaining reduction guide sleeves and into the radius. Plates and screws were applied to the cranial surface of the radius, individually stabilizing each ostectomy. If warranted, an additional plate was contoured and placed on the medial aspect of the radius. Stabilization of the ulna was performed at the discretion of the surgeon. If warranted, cancellous bone graft was harvested from the proximal humerus and packed in any defects. Surgical approaches were closed in routine fashion **(Figure 2)**.

3D assessment

A postoperative CT was acquired, and 3D renderings of the radius in both the VSP and postoperatively were assessed for frontal plane alignment (FPA), sagittal plane alignment (SPA), translation, and antebrachial rotation. Methods outlined by Fox et al[6] were adapted to characterize FPA. Based on previous reports, the target for FPA was 0-8° valgus for nonchondrodystrophic dogs.[6] Sagittal plane alignment was quantified as described by Knapp et al.[16] The defined acceptable range for SPA was 20°

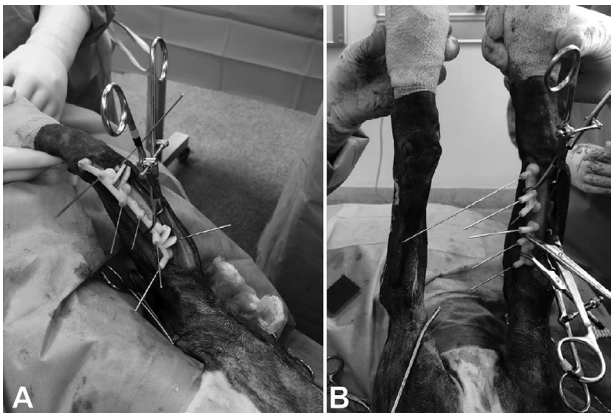

Figure 2—Intraoperative images of a biapical deformity correction (deformity 11) of a dog with an antebrachial deformity of this report. A—The proximal and distal osteotomy guides have been secured to the radius using 1.6 mm Kirschner wires. The reduction forceps were used to maintained proper position of the guides as the Kirschner wires were placed. B—After completion of the osteotomies and removal of the osteotomy guides, the proximal and distal reduction guides were applied to align the radius by means of the original Kirschner wires.

to 32° of procurvatum.[34] Antebrachial rotation was quantified using methods adapted from Fox et al[6] for reference line landmarks. Acceptable rotation was not defined, as our methods differed from previously reported ranges. Translation, or the displacement from the center of the carpus and elbow in the frontal plane, was measured according to methodology described by Dismukes et al.[13]

To assess the accuracy of the surgical procedure with respect to the plan, FPA, SPA, translation and antebrachial rotation were measured on the postoperative CT and compared with the virtual plan. Discrepancies in FPA, SPA, and antebrachial rotation of 5° or less and translation of 5 mm or less between the VSP and postoperative radius were considered acceptable.

Postoperative care and radiographic and clinical assessment

Orthogonal radiographs of the antebrachium were obtained immediately postoperatively and monthly thereafter, until osseous union was confirmed **(Figure 3)**. Limbs were bandaged or splinted for a variable duration at the discretion of the surgeon. Owners were instructed to confine their dog to a crate when unattended and restrict activity to leashed walks until radiographic union of the radial osteotomies was achieved. Follow-up evaluations included direct observation and examination. Postoperative limb function at the time of the final evaluation was graded using the same lameness and conformational and postural criteria as prior to surgery.

Statistical analysis

Preoperative and postoperative limb function was compared in dogs in which guide use was not abandoned using a paired *t* test with a *P* value < 0.05 considered significant.

Results

Dogs

Eleven dogs (thirteen antebrachii) underwent antebrachial deformity correction using the described techniques during the study period. Dogs included mixed breed (n = 4), Beagle (1), Poodle (1), Irish Wolfhound (1), Dachshund (1), Coton de Tulear (1), Shih Tzu (1), and Hound (1). There were 9 male and 2 female dogs, ranging from 6 to 70 kg (median, 15 kg) and aged 12 to 124 months (median, 22 months) at the time of surgery. Nine of the dogs were bilaterally affected, and 2 were unilaterally affected. The mean ± SD preoperative limb function score was 5.2 ± 1.7, and the median score was 6.

Deformities 6 and 8 and deformities 7 and 11 were corrected in the same dog in procedures staged 3 months apart. Seven uniapical and 6 biapical corrections were performed. Ostectomy was planned at the level of the CORA in 3 deformities and translated away from the CORA in 10 deformities. One of the dogs (deformity 4) underwent concurrent pancarpal arthrodesis, with excision of the antebrachiocarpal articular surfaces serving as the distal location of the biapical deformity correction **(Table 1)**.

Surgery and guide use

Osteotomy and reduction guides were successfully used for 11 of the 13 surgeries. Reduction guides were abandoned during 2 surgeries (deformity 2 and 9) due to soft tissue constraints resulting in difficulties in guide placement and limb alignment. In these 2 cases, freehand excision of additional radial segments at the ostectomy sites relieved soft tis-

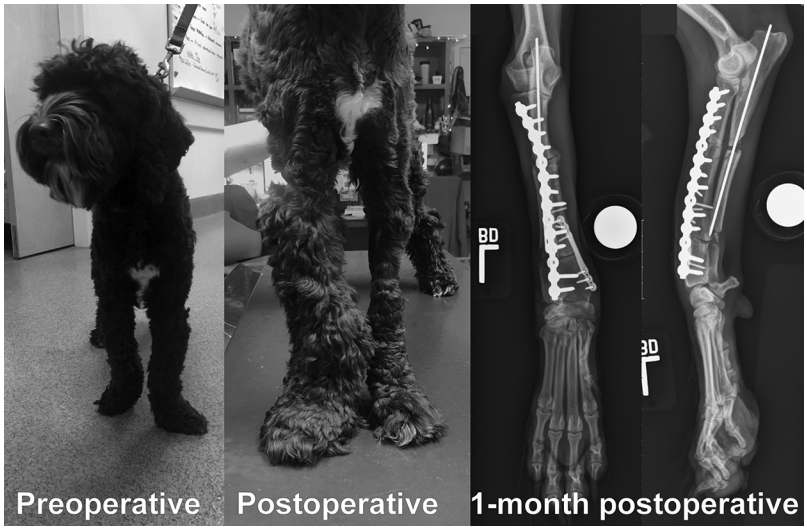

Figure 3—Pre- and postoperative images and 1-month postoperative radiographs of deformity 7 of a dog with an antebrachial deformity of this report.

Table 1—Clinical summaries of deformities (n = 13) that underwent corrective procedures facilitated by 3D virtual surgical planning and 3D printed osteotomy and reduction guides.

Deformity No.	Signalment	Description and etiology of deformity	Procedure	Implants	Intraoperative and postoperative complications	Preoperative and final limb function* (time after surgery)
1	16.7-kg 16-mo-old male Beagle	Unilateral uniapical radial deformity with valgus and external rotation and premature closure of the distal ulnar physis	Left antebrachium: midradial diaphyseal closing wedge ostectomy‡ with rotational, valgus, and procurvatum correction; ulnar diaphyseal osteotomy	Radius: 6-hole, 3.5-mm conical coupling locking plate[a]	None	Preoperative: 1/3 Final: 0/0 (13 mo)
2	7.3-kg 59-mo-old male Dachshund	Bilateral biapical radial deformity with valgus, procurvatum, and external rotation; conformational abnormalities and premature closure of the distal ulnar physis	Right antebrachium: proximal and distal radial closing wedge ostectomies§ with rotational, valgus, and procurvatum correction; proximal and distal ulnar osteotomies†,‖	Radius: 12-hole, 1.5-mm locking compression adaptation plate and 2x 5-hole, 1.7-mm conical coupling locking T-plates[a] Ulna: Intramedullary Kirschner wire	Abandoned guide use due to soft tissue tension; mild proprioceptive deficit long term	Preoperative: 1/3 Final: 1/0 (10 mo)
3	13.8-k 13-mo-old male mixed breed	Bilateral biapical radial deformity with valgus, procurvatum, : and external rotation conformational abnormalities and premature closure of the distal ulnar physis	Left antebrachium: proximal and distal radial closing wedge ostectomies§ with rotational, valgus, and procurvatum correction; proximal ulnar osteotomy†,‖	Radius: 14-hole, 2.0-mm locking compression plate[a] and 2x 5-hole, 1.7-mm conical coupling locking plates[b] Ulna: Intramedullary pin	None	Preoperative: 2/4 Final: 1/2 (8 mo)
4	70.7-kg 60-mo-old male Irish Wolfhound	Bilateral biapical radial deformity with valgus, procurvatum, and external rotation; premature closure of the distal ulnar physis due to retained cartilage core; advanced left carpal degenerative joint disease	Left antebrachium: proximal radial diaphyseal ostectomy and antebrachiocarpal ostectomy§/ arthrodesis with rotational, valgus, and procurvatum correction; proximal and distal ulnar osteotomies‖	Radius: custom 15-hole, 3.5-mm conical coupling plate[a]; 7-hole, 3.5-mm conical coupling pancarpal arthrodesis plate[a]; and 6-hole, 3.5-mm conical coupling plate[a]	Fracture of proximal radius necessitating revision surgery; surgical site infection necessitating implant removal	Preoperative: 3/4 Final:2/2 (6 mo)
5	10.5-kg 50-mo-old male mixed breed	Bilateral biapical radial deformity with valgus, procurvatum, and external rotation; conformational abnormalities and premature closure of the distal ulnar physis	Left antebrachium: midradial diaphyseal closing wedge ostectomy§ with rotational, valgus, and procurvatum correction; ulnar diaphyseal osteotomy	Radius: 7-hole, 2.4-mm locking compression plate[b]	Sensitivity on palpation over radial implants	Preoperative: 1/4 Final: 0/1 (8 mo)
6	11.5-kg 13-mo-old male Poodle	Bilateral external rotational radial and ulnar deformity	Left antebrachium: distal radial diaphyseal ostectomy‡ with rotational correction; ulnar osteotomy‖	Radius: 12-hole, 2.4-mm locking compression plate[b]	Sensitivity on palpation over radial implants	Preoperative: 0/2 Final: 0/0 (14 mo)
7	15.5-kg 21-mo-old male mixed breed	Bilateral biapical radial deformity with valgus, procurvatum, and external rotation conformational abnormalities and premature closure of the distal ulnar physis	Left antebrachium: proximal and distal radial closing wedge ostectomies§ with rotational, valgus, and procurvatum correction; proximal and distal ulnar osteotomies‖	Radius: 14-hole, 2.7-mm string-of-pearls locking plate[c] and 6-hole, 1.7-mm conical coupling locking plate[a] Ulna: Intramedullary pin	Flexure contracture (resolved following flexor carpi ulnaris tenotomy); sensitivity on palpation over radial implants	Preoperative: 2/4 Final: 1/0 (16 mo)
8	11.7-kg 16-mo-old male Poodle	Bilateral external rotational radial and ulnar deformity	Right antebrachium: distal radial diaphyseal ostectomy‡ with rotational correction; ulnar osteotomy‖	Radius: 12-hole, 2.4-mm locking compression plate[b]	None	Preoperative: 0/2 Final: 0/0 (10 mo)
9	27.0-kg 24-mo-old female Hound	Unilateral uniapical radial deformity with distal valgus and external rotation; unknown etiology	Right antebrachium: proximal and distal radial closing wedge ostectomies§ with rotational, valgus, and procurvatum correction; proximal and distal ulnar ostectomies†,‖	Radius: 11-hole, 2.4-mm locking compression plate[b] and 2x 3-hole, 2.5-mm conical coupling plates[a] Ulna: Intramedullary pin	Abandoned guide use due to excessive soft tissue tension; revision surgery performed using a hinged circular external fixator	Preoperative: 3/4 Final: 1/2 (8 mo)
10	23.4-kg 12-mo-old male mixed breed	Bilateral biapical radial deformity with valgus, procurvatum, and external rotation; conformational abnormalities and premature closure of the distal ulnar physis	Left antebrachium: proximal and distal radial closing wedge ostectomies§ with rotational, valgus, and procurvatum correction; proximal and distal ulnar osteotomies†, ‖	Radius: 5-hole, 3.5-mm conical coupling plate[a]; 6-hole, 3.5-mm conical coupling plate[a]; and 14-hole string-of-pearls locking plate[c] Ulna: Intramedullary pin	None	Preoperative: 3/4 Final: 1/2 (14 mo)
11	16.4-kg 33-mo-old male mixed breed	Bilateral biapical radial deformity with valgus, procurvatum, and external rotation; conformational abnormalities and premature closure of the distal ulnar physis	Right antebrachium: proximal and distal radial closing wedge ostectomies§ with rotational, valgus, and procurvatum correction; proximal and distal ulnar osteotomies†,‖	Radius: 13-hole, 2.7-mm string-of-pearls locking plate[c] and 2x 4-hole, 1.7-mm conical coupling plate[a] Ulna: Intramedullary pin	Inadvertent tenotomy of extensor carpi radialis necessitating tenorrhaphy; reduced carpal flexion following coaptation	Preoperative: 2/4 Final: 2/1 (10 mo)
12	5.5-kg 44-mo-old male Coton de Tulear	Bilateral biapical radial deformity with valgus, procurvatum, and external rotation; conformational abnormalities and premature closure of the distal ulnar physis	Right antebrachium: midradial diaphyseal closing wedge ostectomy§ with rotational, valgus, and procurvatum correction; ulnar diaphyseal osteotomy†,‖	Radius: 6-hole, 1.9-mm conical coupling locking plate[a] and 4-hole, 1.9-mm conical coupling locking plate[a] Ulna: Intramedullary pin	None	Preoperative: 2/4 Final:0/0 (9 mo)
13	6.2-kg 23-mo-old female Shih Tzu	Bilateral biapical deformity, with valgus procurvatum, and external rotation; conformational abnormalities and premature closure of the distal ulnar physis	Right antebrachium: midradial diaphyseal closing wedge ostectomy§ with rotational, valgus, and procurvatum correction; ulnar diaphyseal osteotomy†,‖	Radius: 7-hole, 1.7-mm conical coupling locking plate[a] and 4-hole, 1.7-mm conical coupling plate[a]	None	Preoperative: 2/4 Final:1/0 (9 mo)

*Lameness/posture graded on a scale from 0 to 4 as defined in the materials and methods. †Intraoperative fluoroscopy used. ‡Ostectomy located at the center of rotation of angulation. §Ostectomy located remote to the center of rotation of angulation. ‖Cancellous bone graft harvested from proximal humerus implanted at osteotomy site.
[a]DePuy Synthes; Raynham. [b]Fixin; Intrauma. [c]Orthomed; Tigard.

sue tension, and the bone segments were manually reduced for plate application. Guide use was often subjectively easy, but soft tissues sometimes impeded juxta-articular guide placement. This was problematic when extensor tendons interfered with the drill guide towers adjacent to the carpus. Fluoroscopy was used to assess antebrachial alignment during the 2 surgeries in which guide use was abandoned. Fluoroscopy was used to assess implant placement rather antebrachial alignment in 6 additional surgeries (Table 1).

Intra- and postoperative complications

Inadvertent transection of the extensor carpi radialis tendon occurred during correction of deformity 11, and tenorrhaphy was performed. The dog's limb was coapted with the carpus maintained in extension for 6 weeks following surgery. After removal of the splint, the dog had discomfort and reduced range of motion in the carpus..

The proximal radial segment fractured 2 days after surgery in deformity 4. Revision surgery was performed, excising the proximal portion of the cranial plate and explanting the proximal medially positioned plate. A 3.5-mm locking compression plate (LCP; DePuy Synthes) extending from the lateral surface of the proximal ulna to the distolateral aspect of the ulna and the radius was placed for supplemental fixation. A plate was also placed laterally, bridging the proximal and central radial segments. Following the revision surgery, ischemic skin necrosis developed over the lateral aspect of the distal ulna and carpus, exposing the distal portion of the plate. The resultant wound cultured positive for mixed enteric bacteria and was managed conservatively with bandaging and enrofloxacin and cephalexin administra-

tion. Implants were removed 4 months after initial surgery once osseous union had been achieved.

Reduced carpal extension was noted initially in deformity 2, but extension improved with daily exercises consisting of forced flexion and extension of the elbow and carpal joints. Immediately following surgery, deformity 7 had markedly reduced carpal extension, which was a source of lameness and did not resolve with conservative management. One month after surgery, the performance of flexor carpi ulnaris muscle tenotomy restored carpal extension and resolved the dog's lameness. When the dog subsequently had surgery on the contralateral limb (deformity 11), preemptive flexor carpi ulnaris tenotomy was performed.

Two dogs (deformities 5 and 6) showed a mild pain response when pressure was applied to their implants without overt clinical or radiographic evidence of infection. Their owners perceived that the implants were a source of discomfort and the cause of intermittent lameness. The plate and screws were explanted 3 months after surgery in 1 dog (deformity 5). Deformities 6 and 8 (affecting the same dog) had implants removed from both limbs in a single session performed 6 and 10 months postoperatively from their respective index surgery. Clinical abnormalities resolved in both dogs following implant removal.

Accuracy and alignment

Postoperative CT data were available for 10 of 13 deformities. Postoperative CT data were not obtained for the 2 deformities in which reduction guide use was abandoned (deformities 2 and 9) or for the deformity that fractured postoperatively (deformity 4).

All frontal and sagittal plane alignment comparisons between the VSP and postoperative limbs met the criteria for acceptable accuracy within 5° variation. Nine of 10 limbs were under the 5° threshold for variation in rotation, and 8 of 10 corrected radii were translated to within 5 mm of the VSP. Of the above measured parameters evaluated, 91.6% met our criteria of acceptable accuracy of 5° and 5 mm variation between corrected limb and VSP **(Table 2)**.

The mean ± SD postoperative valgus was 6 ± 4°, procurvatum was 26 ± 7°, and antebrachial rotation was 18 ± 7°. Valgus exceeded the reference range in 2 out of 10 postoperative limbs, and procurvatum exceeded the reference range for 3 out of 10 postoperative limbs. Of the parameters that were outside the reference range on postoperative limbs, the VSP was also outside the defined range **(Table 3)**.

Radiographic and clinical outcome

All dogs achieved radiographic osseous union of radial ostectomies within 12 weeks after surgery (Table 1). At the time of the final assessment (range, 6 to 16 months; median, 10 months following surgery), the mean ± SD limb function scores for the 10 limbs in which guides were used had improved significantly (P = 0.0001) from 5 ± 1.8 to 1.2 ± 1.3.

Table 2—Discrepancies in alignment parameters between the virtual surgical plan and the postoperative CT. An acceptable result was defined as alignment within ≤ 5° or ≤ 5 mm of the virtual surgical plan (n = 10).

Deformity No.	Frontal plane angulation (valgus)	Sagittal plane angulation (procurvatum °)	Antebrachial rotation (external °)	Mediolateral translation (axial mm)
1	1	2	1	1
3	1	4	4	12
5	1	1	3	1
6	1	4	2	1
7	1	2	5	5
8	2	1	5	3
10	2	2	7	10
11	4	2	3	3
12	3	2	4	2
13	2	5	1	4

Table 3—Summary of pre- and postoperative limb alignment in deformities that had postoperative CT (n = 10).

Deformity No.	Frontal plane angulation (valgus °)		Sagittal plane angulation (procurvatum °)		Antebrachial rotation (external °)	
	Preoperative	Postoperative	Preoperative	Postoperative	Preoperative	Postoperative
1	28	7	51	28	66	32
3	40	1	42	26	86	8
5	31	12	45	23	59	29
6	9	3	16	15	47	15
7	31	1	46	22	40	18
8	7	2	17	16	45	16
10	53	3	41	32	30	19
11	34	7	54	23	36	17
12	42	13	75	36	48	15
13	38	8	68	35	42	17

Discussion

This retrospective case series describes and evaluates our initial clinical experiences utilizing VSP and 3D custom guide printing to correct uni- and biapical antebrachial deformities in dogs. Virtual 3D models of the thoracic limbs were generated from CT scans, and 3D medical imaging and design software were used to develop a VSP for each deformity. Custom osteotomy and reduction guides were designed and 3D printed to execute the virtual plan. The guides were used according to plan in 11 out of 13 deformity surgeries. Of the 10 deformities with postoperative CT, accuracy of all alignment parameters was acceptable. Alignment and posture were improved in all limbs. While there is substantial latitude for further development of this new technique, we feel that the osteotomy and reduction guides, as well as the printed VSP bone models, greatly facilitated these procedures.

Previous reports describing VSP of deformity corrections in dogs involved translating joint reference planes to converge at the CORA to determine the magnitude of the angle for a closing wedge ostectomy[18] or calculation of the magnitude of angles based off of virtual correction.[19,26,28] We visually determined the number and locations of the CORAs to establish how and where to perform the osteotomies.[6,26,35] The distal radial segments were virtually angulated, rotated, and translated in 3D space until the distal radius and manus were axially aligned with the distal humerus in the frontal plane; procurvatum was reduced and antebrachial rotation was resolved.[26] Once the corrected limb was finalized and overlapping segments were removed, the corrected virtual radius was used to create reduction guides, and the corrected radial segments were translated to the precorrection limb to derive the osteotomy guides. Carwardine et al[28] employed a visual virtual correction but used the correction to calculate the angle or magnitude of the wedge ostectomy. In our method, the CORA's magnitude was not definitively calculated in any plane; rather, we virtually aligned the proximal and distal segments, which determined the ostectomy configurations. This allowed complex, multiplanar corrections to be designed easily, including biapical corrections. Another advantage of the visual correction described here and by Carwardine et al[28] is that alignment is less affected by degenerative or dysplastic articular abnormalities that are often present in dogs with limb deformities.[8,13,16,18] While computer-aided design software and 3D printing require advanced training and experience, our retrograde visual deformity correction process, using the final corrected limb model to subsequently design the guides, is intuitive—even when the deformity is complex.

Guides were successfully used in 11 out of 13 corrective surgeries. Deformity correction can increase functional limb length, even when closing wedge ostectomies are performed.[12] Substantial soft tissue tension can develop in response to acute functional lengthening and forced us to abandon use of the reduction guide in deformities 2 and 9. Soft tissue tension was also problematic during reduction as well as during the postoperative convalescent period in deformity 8, and a flexor carpi ulnaris tenotomy was eventually required to allow functional extension of the carpus. In planning deformity corrections subsequent to those reported here, we began incorporating limb segment shortening into the closing wedges if the magnitude of the CORA was high to reduce soft tissue tension. We also noted that properly executing narrow wedge ostectomies was challenging due to the limited space between osteotomy shelves. Segment shortening may facilitate wedge ostectomies by widening the space for saw blade placement between the osteotomy shelves.

Deformities with juxta-articular CORAs presented a number of challenges, particularly in small dogs. Obtaining sufficient exposure of the radius for accurate guide application near the elbow and carpus was difficult. The physical application of implants when stabilizing a juxta-articular osteotomy is also challenging, and plates and screws adjacent to the carpus can potentiate lameness.[11] This was likely a source of persistent lameness in 2 dogs (deformities 5 and 6) in our study. As we gained experience, we began translating osteotomies away from elbow and carpus if a CORA was positioned in a periarticular location (deformities 12 and 13), necessitating compensatory translation of the distal segment at the level of the ostectomy.[12] Deformities 12 and 13 were biapical deformities in dogs weighing < 7 kg. Even if we moved the location of the osteotomies more centrally, away from the CORA, the resultant proximal and distal radial segments would have been very short, making plate application difficult. We elected to perform a central uniapical correction in these smaller radii to allow room for fixation. The more centralized, shortening uniapical correction performed in deformities 12 and 13 also mitigated tension when realigning the radial segments. These findings led the authors to consider performing a uniapical correction to address biapical deformities in very small dogs.

Postoperative complications in this study included implant failure necessitating revision surgery with resultant infection (deformity 4) and implant irritation (deformities 5 and 6), which was not attributed to 3D VSP and guide use. Our results are comparable to those of other reports[18,26] describing the use of 3D custom guides for antebrachial deformity corrections in dogs. Worth et al[18] reported guide use in 7 antebrachial deformity corrections. Of the 7, one dog required revision due to residual deformity and another dog required revision surgery because of implant failure. Carwardine et al[28] did not report any complications, but this study only involved 4 dogs.

In the 10 dogs in which postoperative CT was performed, > 90% of parameters assessed on our postoperative limb analysis were accurate when compared with the virtual plan using the defined criteria. These findings corroborate a high degree of accuracy associated with the use of 3D guides for deformity corrections in previous veterinary studies.[18,22,26] Hall et al[22] describe the use of vir-

tual planning and custom 3D printed guides for performing distal femoral ostectomies in dogs with medial patella luxation, a procedure that typically addresses a uniapical deformity correction with fewer inherent challenges than the antebrachial deformities reported here. Hall et al[22] reported 66% accuracy between their postoperative result and the virtual plan, but the defined range of acceptability was smaller, within 2°, than our study. Carwardine et al[28] reported an average angular difference of 3.5° in the frontal plane and 7.5° in the sagittal plane between the virtual plan and the postoperative result in a series of 4 antebrachial deformity corrections using custom 3D printed guides. Our accuracy is similar to that reported by Carwardine et al despite the majority of our cases being biapical corrections, whereas Carwardine et al reported only uniapical corrections. The study by Carwardine et al[28] also used custom 3D printed plates. Plates designed for a specific VSP may improve accuracy; however, we were able to achieve similar results with commercially available plates and screws. Contouring plates to conform to printed models of the corrected radius likely contributed to the surgical accuracy. Inaccuracies may originate during guide fabrication, errors in guide application, and osseous displacement during fixation. While assessing these potential issues was beyond the scope of this study, it is worth exploring in future studies using custom surgical guides.

When comparing the postoperative limbs to previously reported alignment parameters,[6,34] 2 dogs (deformities 5 and 12) had residual valgus, and 2 dogs (deformities 12 and13) had residual procurvatum. These parameters, however, were accurate to within 5° of the VSP and reflect the accepted planned results made by the surgeon on these cases. All 3 of these were biapical cases that underwent uniapical corrections. These dogs were chondrodystrophic, were small, and had short radii, and leaving some degree of residual deformity was considered acceptable.

A combined score evaluating both lameness and conformation and posture was used to assess limbs pre- and postoperatively. The scoring was improved in all cases postoperatively. Other methods of assessment were used, but similar improvement and favorable clinical outcome have been reported when using 3D VSP and surgical guides.[26]

Cosmesis was suboptimal in deformity 11. In this limb, the proximal radial head was externally rotated and laterally subluxated. The virtual surgical plan assumed that elbow congrency would improve following ulnar osteotomy in surgery. Postoperative 3D comparison between the virtual plan and postoperative limb confirmed that the radial head did not reduce as was assumed in the virtual plan. Kwan et al[10] noted that radial head subluxation did not seem to be improved following deformity correction, but could not confirm due to lack of postoperative CT data. Our postoperative analysis corroborates the supposition that the radial head position remains unchanged after correction.

Limitations of this study are primarily its retrospective nature and the small number of procedures. Our VSP methodology and guide design evolved with experience during the 2-year study period. Our target alignment was subjective and varied among the surgeons responsible for individual cases. Tangible comparisons of our results with those of previously described surgical techniques for correcting antebrachial deformities was not possible due to variability in study design and reported outcome measures.[1–11] A prospective study would yield more consistent and objective preoperative and long-term functional outcome measures and could be designed to compare the efficacy of VSP and the use of printed guides to alternate described methods for performing deformity corrections.

This case series represents our initial experiences of utilizing VSP and printing custom guides to facilitate both uni- and biapical antebrachial deformity corrections at our institution. We utilized a unique VSP to design reduction and osteotomy guides. Our postoperative CT results confirmed a high degree of accuracy in executing the virtual surgical plan. As this technology is adopted by more small animal surgeons, future studies should aspire to refine these preoperative planning techniques, guide design, and application. Presumably, this technology could also be employed in correlating postoperative morphologic results with functional outcomes. Additionally, prospective evaluation of these methods may prove useful when comparing VSP and the use of patient-specific guides with more traditional approaches to limb deformity correction.

Acknowledgments

Supported by the University of Florida, College of Veterinary Medicine's Mark S. Bloomberg Memorial Small Animal Surgery Resident Research Fund.

The authors have no other conflicts of interest or funding to declare relating to this report.

References

1. MacDonald JM, Matthiesen D. Treatment of forelimb deformity in 11 dogs by radial dome osteotomy and external coaptation. *Vet Surg*. 1991;20(6):402–408. doi:10.1111/j.1532-950x.1991.tb00347.x
2. Fox SM, Bray JC, Guerin SR, Burbridge HM. Antebrachial deformities in the dog: treatment with external fixation. *J Small Anim Pract*. 1995;36(7):315–320. doi:10.1111/j.1748-5827.1995.tb02936.x
3. Marcellin-Little DJ, Ferretti A, Roe SC, DeYoung DJ. Hinged Ilizarov for correction of antebrachial deformities. *Vet Surg*. 1998;27(3):231–245. doi:10.1111/j.1532-950x.1998.tb00122.x
4. Lewis DD, Radasch RM, Beale BS, et al. Initial clinical experience with the IMEX Circular External Skeletal Fixation System. Part II: use for bone lengthening and correction of angular and rotational deformities. *Vet Comp Orthop Traumatol*. 1999;12(3):118–127. doi:10.1055/s-0038–1632476
5. Balfour RJ, Boudrieau RJ, Gores BR. T-plate fixation of distal radial closing wedge osteotomies for treat-

ment of angular limb deformities in 18 dogs. *Vet Surg*. 2000;29(3):207–217. doi:10.1053/jvet.2000.4396
6. Fox DB, Tomlinson JL, Cook JL, Breshears LM. Principles of uniapical and biapical radial deformity correction using dome osteotomies and the center of rotation of angulation methodology in dogs. *Vet Surg*. 2006;35(1):67–77. doi:10.1111/j.1532-950X.2005.00114.x
7. Sereda CW, Lewis DD, Radasch RM, Bruce CW, Kirkby KA. Descriptive report of antebrachial growth deformity correction in 17 dogs from 1999–2007, using hybrid linear-circular external fixator constructs. *Can Vet J*. 2009;50(7):723–732.
8. Crosse KR, Worth AJ. Computer-assisted surgical correction of an antebrachial deformity in a dog. *Vet Comp Orthop Traumatol*. 2010;23(5):354–361. doi:10.3415/VCOT-10-01-0010
9. Fitzpatrick N, Nikolaou C, Farrell M, et al. The double-arch modified type-1b external skeletal fixator. *Vet Comp Orthop Traumatol*. 2011;24(5):374–382. doi:10.3415/VCOT-10-06-0086
10. Kwan TW, Marcellin-Little DJ, Harrysson OL. Correction of biapical radial deformities by use of bi-level hinged circular external fixation and distraction osteogenesis in 13 dogs. *Vet Surg*. 2014;43(3):316–329. doi:10.1111/j.1532-950X.2014.12114.x
11. Kim SY, Snowdon KA, DeCamp CE. Single oblique osteotomy for correction of antebrachial angular and torsional deformities in a dog. *J Am Vet Med Assoc*. 2017;251(3):333–339. doi:10.2460/javma.251.3.333
12. Paley D. Osteotomy concepts and frontal plane realignment. In: Paley D, Herzenberg JE, eds. *Principles of Deformity Correction*. Springer; 2002:99–154.
13. Dismukes DI, Fox DB, Tomlinson JL, Essman SC. Use of radiographic measures and three-dimensional computed tomographic imaging in surgical correction of an antebrachial deformity in a dog. *J Am Vet Med Assoc*. 2008;232(1):68–73. doi:10.2460/javma.232.1.68.
14. Radasch RM, Lewis DF, McDonald DE, Calfee EF, Barstad RD. Pes varus correction in Dachshunds using a hybrid external fixator. *Vet Surg*. 2008;37(1):71–81. doi:10.1111/j.1532-950X.2007.00350.x
15. Meola SD, Wheeler JL, Rist CL. Validation of a technique to assess radial torsion in the presence of procurvatum and valgus deformity using computed tomography: a cadaveric study. *Vet Surg*. 2008;37(6):525–529. doi:10.1111/j.1532-950.2008.00399.x
16. Knapp JL, Tomlinson JL, Fox DB. Classification of angular limb deformities affecting the canine radius and ulna using the center of rotation of angulation method. *Vet Surg*. 2016;45(3):295–302. doi:10.1111/vsu.12460
17. Piras LA, Peirone B, Fox D. Effects of antebrachial torsion on the measurement of angulation in the frontal plane: a cadaveric radiographic analysis. *Vet Comp Orthop Traumatol*. 2012;25(2):89–94. doi:10.3415/VCOT-10-09-0135
18. Worth AJ, Crosse KR, Kersley A. Computer-assisted surgery using 3D printed saw guides for acute correction of antebrachial angular limb deformities in dogs. *Vet Comp Orthop Traumatol*. 2019;32(3):241–249. doi:10.1055/s-0039-1678701
19. Miyake J, Murase T, Oka K, Moritomo H, Sugamoto K, Yoshikawa H. Computer-assisted corrective osteotomy for malunited diaphyseal forearm fractures. *J Bone Joint Surg Am*. 2012;94(20):e150. doi:10.2106/JBJS.K.00829
20. Oxley B. Bilateral shoulder arthrodesis in a Pekinese using three-dimensional printed patient-specific osteotomy and reduction guides. *Vet Comp Orthop Traumatol*. 2017;30(3):230–236. doi:10.3415/VCOT-16-10-0144
21. Fujioka T, Nakata K, Nishida H, et al. A novel patient-specific drill guide template for stabilization of thoracolumbar vertebrae of dogs: cadaveric study and clinical cases. *Vet Surg*. 2019;48(3):336–342. doi:10.1111/vsu.13140
22. Hall EL, Baines S, Bilmont A, Oxley B. Accuracy of patient-specific three-dimensional-printed osteotomy and reduction guides for distal femoral osteotomy in dogs with medial patella luxation. *Vet Surg*. 2019;48(4):584–591. doi:10.1111/vsu.13126
23. Hamilton-Bennett SE, Oxley B, Behr S. Accuracy of a patient-specific 3D printed drill guide for placement of cervical transpedicular screws. *Vet Surg*. 2018;47(2):236–242. doi:10.1111/vsu.12734
24. Lam G, Kim SY. Three-dimensional computer-assisted surgical planning and use of three-dimensional printing in the repair of a complex articular femoral fracture in a dog. *Vet Comp Orthop Traumatol*. 2018;1(1):e12–e18. doi:10.1055/s-0038–1676062
25. Oxley B. 3-dimensional-printed patient-specific guide system for minimally invasive plate osteosynthesis of a comminuted mid-diaphyseal humeral fracture in a cat. *Vet Surg*. 2018;47(3):445–453. doi:10.1111/vsu.12776
26. Shi J, Lv W, Wang Y, et al. Three-dimensional patient-specific printed cutting guides for closing-wedge distal femoral osteotomy. *Int Orthop*. 2019;43(3):619–624. doi:10.1007/s00264-018-4043-3
27. Lynch AC, Davies JA. Percutaneous tibial fracture reduction using computed tomography imaging, computer modelling and 3D printed alignment constructs: a cadaveric study. *Vet Comp Orthop Traumatol*. 2019;32(2):139–148. doi:10.1055/s-0039-1677751
28. Carwardine DR, Gosling MJ, Burton NJ, O'Malley FL, Parsons KJ. Three-dimensional-printed patient-specific osteotomy guides, repositioning guides and titanium plates for acute correction of antebrachial limb deformities in dogs. *Vet Comp Orthop Traumatol*. 2021;34(1):43–52. doi:10.1055/s-0040-1709702
29. Mulford JS, Babazadeh S, Mackay N. Three-dimensional printing in orthopaedic surgery: review of current and future applications. *ANZ J Surg*. 2016;86(9):648–653. doi:10.1111/ans.13533
30. Green N, Glatt V, Tetsworth K, Wilson LJ, Grant CA. A practical guide to image processing in the creation of 3D models for orthopedics. *Tech Orthop*. 2016;31(3):153–163. doi:10.2147/ORR.S99614
31. Tetsworth KD, Mettyas T. Overview of emerging technology in orthopedic surgery: what is the value in 3D modeling and printing? *Tech Orthop*. 2016;31(3):143–152. doi:10.1097/BTO.0000000000000187
32. Zhang YZ, Sheng L, Chen B, Zhao JM, Liu R, Pei GX. Application of computer-aided design osteotomy template for treatment of cubitus varus deformity in teenagers: a pilot study. *J Shoulder Elbow Surg*. 2011;20(1):51–56. doi:10.1016/j.jse.2010.08.029
33. Johnson KA. *Piermattei's Atlas of Surgical Approaches to the Bones and Joints of the Dog and Cat*. 5th ed. Elsevier Saunders; 2014:322–328.
34. Fasanella FJ, Tomlinson JL, Welihozkiy A. Radiographic measurements of the axes and joint angles of the canine radius and ulna. *Vet Comp Orthop Traumatol*. 2010;20(23):25. 37th Annual Conference of the Veterinary Orthopedic Society abstract A11.
35. Fox DB, Tomlinson JL. Principles of angular limb deformity correction. In: Johnston SA, Tobias KM, eds. *Veterinary Surgery: Small Animal*. 2nd ed. Elsevier; 2018:762–774.